A high-resolution timescale for the Miocene Shanwang diatomaceous shale lagerstätte (China)

Yu, Jifeng; Pang, Xinlong; Fu, Wenzhao; Hilton, Jason; Liang, Mingmei; Jiang, Zongkai ; Zhao, Xiuli ; Qiao, Wenyan ; Shi, Suo ; Zhang, Diandong ; Cao, Huitao ; Jia, Haibo ; Wang, Yadong ; Hu, Xiaoke ; Zhang, Rui

DOI:
10.1007/s12303-020-0055-2

A high-resolution timescale for the Miocene Shanwang diatomaceous shale lagerstätte (China): development of Wavelet Scale Series Analysis for cyclostratigraphy

Jifeng Yu[a, b,*], Xinlong Pang[a], Wenzhao Fu[c], Jason Hilton[d], Mingmei Liang[d], Zongkai Jiang[a], Xiuli Zhao[a], Wenyan Qiao[a], Suo Shi[a], Diandong Zhang[a], Huitao Cao[a], Haibo Jia[a], Yadong Wang[a], Xiaoke Hu[a], Rui Zhang[e]

[a] Shandong University of Science and Technology, Qingdao 266590, Shandong, China

[b] Laboratory for Marine Mineral Resources, Qingdao National Laboratory for Marine Science and Technology, Qingdao 266235, Shandong, China

[c] Liaoning Technical University, Fuxin 123000, Liaoning, China

[d] School of Geography, Earth and Environmental Sciences, University of Birmingham, Edgbaston, Birmingham, B15 2TT, UK

[e] China University of Petroleum, Qingdao 266580, Shandong, China

* Corresponding author at: Shandong University of Science and Technology, Qingdao 266590, Shandong, China. Tel:+86-13869880455

E-mail address: yujifeng05@126.com (J.Y.), pangxinlong@sina.com (X.P.), fwz04@163.com (W.F.), j.m.hilton@bham.ac.uk (J.H.), 2586833166@qq.com (Z.J.), 272219245@qq.com (X.Z.), 707286496@qq.com (W.Q.), 1027054698@qq.com (S.S.), 1797176268@qq.com (D.Z.), 1530547140@qq.com (H.C.), jiahaibohb@163.com (H.J.), 736145499@qq.com (Y.W.), 18395577837@163.com (X.H.), 1139365064@qq.com (R.Z.)

ABSTRACT

The Miocene aged Shanwang Formation from the Shanwang National Geopark in China represents a succession of lacustrine diatomaceous shales containing an abundant and diverse biota with lagerstätte fossilization of soft tissues. To date, the Shanwang Formation has not been investigated for cyclostratigraphy nor has it been dated with high precision methods. Now we use thorium data as a paleoenvironmental and paleoclimatic proxy to conduct a detailed cyclostratigraphic analysis. A new and simple cyclostratigraphic method, Wavelet Scale Series Analysis (WSSA), using the Wavelet Analysis toolbox in Matlab, is developed to recognize Milankovitch cycles. A total of three short eccentricity and fifteen precession cycles are identified; obliquity cycles are not apparent. In the sedimentary succession, the corresponding precession and short eccentricity cycles are 1.17 m and 4.98 m thick respectively, with this verified by Correlation Coefficient (COCO) analysis and Multitaper-Method (MTM) spectral analysis. We estimate the studied interval was deposited over a duration of 0.3 Myr with a depositional rate of c. 5.7 cm/kyr. Paleomagnetic and radio isotope dating data shows that the diatomaceous shale was deposited during Chron C5En, which places it at approximately 18.5 Ma during the Burdigalian stage of the Early Miocene, rather than in the Middle Miocene as previously thought. The Shanwang lagerstätte biota therefore predates the Middle Miocene Climate Optimum (MMCO) and did not form within it. The geological time scale with a high resolution of 20 kyr was set accordingly.

Key words: Milankovitch cycles, Spectral analysis, Geochronology, Chron C5En, Burdigalian

1. INTRODUCTION

The Shanwang Formation in the Shanwang National Geopark (Shandong Province, E China) comprises a succession of diatomaceous shales that formed in a small inland basin during the Miocene (Liang et al., 2003). The Shanwang site is world famous because of the diversity of fossils it contains, and because of their exceptional preservation, representing a rare occurrence of lagerstätte grade fossilization of soft tissues (e.g., Seilacher et al., 1985) from the Miocene (Yang and Yang, 1994). This can be compared favorably with Germany's famous Jurassic aged Solenhofen Limestone site in terms of its scientific importance (Holden, 2001).

The majority of past research on the Shanwang Formation has focused on taxonomic and systematic investigations of its fossils that have supported various palaeoecological and palaeoclimate investigations (e.g., Yang and Yang, 1994; Sun et al., 2002; Liang et al., 2003). Li et al. (1984) used the Shanwang fauna to define one of the Eastern Asian Land Mammal Ages of the Neogene, designating from it the Shanwangian Stage that has been widely adopted by paleontologists subsequently. He et al. (2011) undertook $^{40}Ar/^{39}Ar$ dating of the basalts in the Shanwang Basin and determined those below the Shanwang Formation formed at 21.0 ± 2.5 Ma with a total age range of 18.5–23.5 Ma, while those above the Shanwang Formation formed at 17.3 ± 1.4 Ma with a total range of 15.9–18.7 Ma. These radiometric age ranges are broad and lack precision for determining the absolute age and rates of deposition for the Shanwang Formation. Research into Milankovitch cyclicity has not been undertaken thus far on the Shanwang Formation, nor has a high-resolution time scale for the succession been established. This restricts deep time climate studies of this stratigraphic interval to some extent, although more recently new paleoclimate classifications have been proposed to bridge the gap between modern and deep time climate studies (e.g., Zhang et al., 2015).

As a newly developed non-biostratigraphic dating tool, cyclostratigraphy can provide a high-resolution astronomical time scale (ATS) by tuning the cyclic stratigraphic records to astronomical solutions (Hinnov and Ogg, 2007; Hilgen et al., 2010; Batenburg et al., 2012; Wu et al., 2014). Here we present a high-resolution cyclostratigraphic analysis of the lagerstätte-bearing diatomaceous shales in the Shanwang Basin for the first time, using thorium (Th) logging data. The main objective of the present contribution is to provide a high-resolution geological time scale for the diatomaceous shales in order to precisely date the Shanwang Formation, and to determine the duration of its accumulation.

2. LOCATION AND GEOLOGICAL SETTING

The Shanwang Basin (36°N,118°E) is located 22 km northeast of Linqu County in the centre of Shandong Province, eastern China, adjacent to the Tan-Lu Fault Zone (Fig. 1a). It is a small maar lake basin formed in a volcanic crater that is oriented from northwest to southeast with an area less than 1 km^2 (Zhang and Shan, 1994).

The Miocene sediments in the basin from the bottom to the top comprise the Niushan, Shanwang and Yaoshan formations. The thickness of each of the Niushan and Yaoshan formations are over 100 m, while the total thickness of the Shanwang Formation is ~100m. The Shanwang Formation is divided into six units. These are a yellow sandstone and tuff breccia at the bottom (Unit1), which only occur at the edges of the basin and have an unconformable contact with Niushan Formation. The middle part of the formation (Unit 2) comprises gray and white diatomaceous shale, interspersed with multiple layers of tuff, phosphorus nodules and marl. The upper part of the

Formation (Units 3–6) comprises green mudstone, brown carbonaceous mudstone, interspersed with two layers of basalt and apical sandstone (Fig. 1b). Our study deals with unit 2 from the Shanwang Formation, which is the main diatomaceous succession containing abundant and well-preserved fossils that comprises the principle unit of the fossil lagerstätten (Fig. 1c). The main lithology of the studied section is diatomaceous shale, which is mainly composed of siliceous diatom and radiolarian fossils, in addition to clay minerals and organic matter (Qin et al., 2004; Yu et al., 2017). The color of the diatoms and radiolarians is typically white and brighter than that of the clay and organic matter. Consequently, sediment color depends largely on the siliceous microfossil content; the more diatoms and radiolarians are present, the brighter colored the sediment becomes (Fig. 2).

Approximate position of Fig. 1

Approximate position of Fig. 2

3. DATA AND METHODS

3.1. Data Collection and Selection

Data most commonly used to study Milankovitch cycles in sediments are usually from lithological outcrop or borehole cores. Methods typically use colour variation (e.g. gray values from profile images), gamma ray logs, magnetic susceptibility, Total Organic Carbon (TOC) content, or carbonate content of samples amongst other proxies (e.g., Prokoph and Barthelmes, 1996; Husson et al., 2011; Batenburg et al., 2012; Pas et al., 2018). For this study, spectral gamma-ray (SGR) values were measured in situ with a portable “GS-512” gamma spectrometer with evenly spaced sampling intervals of 5 cm and vertically through the measured profile of Unit 2. This method is a quick and simple, yet powerful technique to better correlate well data with surface geology (Aigner et al., 1995).

SGR data relating to the amount of radioactive potassium (K), uranium (U) and thorium (Th) in rocks have been widely used in paleoclimatic and paleoenvironmental research (Wu et al., 2009; Zhang et al., 2010). Levels of K, U and Th vary within sedimentary rocks. K is common in sediments containing feldspar, mica, clays or salts, while U and Th have a number of host minerals in sedimentary rocks including clays, feldspars, heavy minerals, phosphates and organic matter. K is leached from feldspars and muscovite during kaolinite formation under conditions of hot and humid climates, while Th is at least partially insoluble and concentrates during weathering (Parkinson, 1996; Osmond and Ivanovich, 1992). U is more soluble than Th and thus prone to mobilisation during leaching and clay mineral diagenesis.

Th logging data are considered to be more stable than K and U, and have been widely used as a palaeoclimate indicator in previous studies. For example, Wu et al. (2013) used the Th logging data from the Yaojia Formation to track lithological change, with high Th occurring in mudstones and low Th in sandstones. In lacustrine sediments, higher Th values are related to higher content of clay minerals and organic carbon, which may have resulted from wetter and warmer climate conditions. Wet periods may have enhanced chemical weathering and clay mineral inputs, nutrient input and higher productivity in the paleolakes, resulting in high values. Conversely, decreased chemical weathering during dry periods may correspond to the negative peaks of Th values (Wu et al., 2009; Wang et al., 2013). Wu et al. (2014) also used thorium (Th) logging data as a paleoenvironmental and paleoclimatic proxy to conduct a detailed cyclostratigraphic study of the core from well SK-1n in

Songliao Basin northeastern China. For these reasons, the Th data series was selected in this study as the most reliable paleoclimatic and paleoenvironmental proxy for cyclostratigraphic analysis (Fig. 3a).

3.2. Data Analysis Method (WSSA)

In the development of cyclostratigraphy, various different methods for spectral analysis have been used to extract Milankovitch cyclicity within a time series of different geological signals, including Fourier Transform (Park and Herbert, 1987; Wu et al., 2014), WALSH transform (Weedon, 1986, 1989), maximum entropy spectrum analysis (Hinnov and Goldhammer, 1991; Dimri and Prakash, 2001), and wavelet analysis (Prokoph and Barthelmes, 1996; Torrence and Compo, 1998). Other methods including the neural estimator, PCA-Music method and the genetic algorithm (GA) have also been introduced into this area (Tagliaferri et al., 2001), as have new methods or computer packages such as the COCO (Correlation Coefficient) and MTM (Multitaper-Method spectral analysis) (Thomson, 1982; Paillard et al., 1996; Ghil et al., 2002; Li et al., 2018).

Wavelet transform theory is a new signal processing technology developed in recent decades (Mallat, 1989; Chui, 1992). Because of its high resolution in both time and frequency domains, it is informally termed the "mathematical microscope" and widely used in numerical signal processing fields (James and Michael, 2006; Yu et al., 2010). As a method, it has been applied to the recognition of Milankovitch cycles in different ways by previous researchers (e.g. Prokoph and Agterberg, 1999, 2000; Yu et al., 2008; Batenburg et al., 2012). There are two kinds of wavelet transform, namely, the Continuous Wavelet Transform (CWT) and Discrete Wavelet Transform (DWT). CWT involves a transform from a one-dimensional time series (or frequency spectrum) to a diffuse two-dimensional time–frequency image of the wavelet coefficient called scalogram, produced through the convolution of a basic wavelet function $\Psi_{a,b}(x)$, with the analyzed signal *f(x), a, b* representing the scale factor and shift factor of the basic wavelet function respectively (Fig. 3b; Eq. 1). Usually the Morlet wavelet is selected as the basic wavelet function in CWT, because the shape of this basic function is similar to a sinusoid function, which allows interpretations of repeat time series and its sinusoidal shape makes it particularly suitable for sedimentary cycles without well-defined shapes (Prokoph and Agterberg, 2000). CWT was once regarded as an interesting diversion that produces colorful pictures that were purely qualitative results because of the misconception of CWT itself. Here we propose a new quantitative method, Wavelet Scale Series Analysis (WSSA), to extract periodic information within time series of paleoclimate proxies, and apply this to the recognize Milankovitch-cycle from Thorium data. This method requires the following six steps.

(1) Do CWT to calculate the wavelet coefficient matrix of a signal $f(x) \in L^2(R)$:

$$\mathrm{CWT}_{a,b} = \int_R f(x)\overline{\psi_{a,b}(x)}dx = |a|^{-\frac{1}{2}}\int_R f(x)\overline{\psi(\frac{x-b}{a})}dx, \quad (1)$$

to get the wavelet coefficient matrix $C_{a,b}$:

$$C_{a,b} = \begin{bmatrix} C_{a_1b_1} & C_{a_1b_2} & \cdots & C_{a_1b_n} \\ C_{a_2b_1} & C_{a_2b_2} & \cdots & C_{a_2b_n} \\ \vdots & \vdots & \ddots & \vdots \\ C_{a_mb_1} & C_{a_mb_2} & \cdots & C_{a_mb_n} \end{bmatrix}. \quad (2)$$

(2) Calculate the absolute value of the wavelet coefficient matrix to form a new matrix:

$$C_{i,j}=\left|C_{a,b}\right|=\begin{bmatrix} \left|C_{a_1b_1}\right| & \left|C_{a_1b_2}\right| & \cdots & \left|C_{a_1b_n}\right| \\ \left|C_{a_2b_1}\right| & \left|C_{a_2b_2}\right| & \cdots & \left|C_{a_2b_n}\right| \\ \vdots & \vdots & \ddots & \vdots \\ \left|C_{a_mb_1}\right| & \left|C_{a_mb_2}\right| & \cdots & \left|C_{a_mb_n}\right| \end{bmatrix}. \tag{3}$$

(3) Calculate the mean value of each row of the new matrix to get a vector, a scale series:

$$\overline{C_{\mathrm{i}}}=\begin{bmatrix} \sum C_{1\mathrm{j}}/\mathrm{n} \\ \sum C_{2\mathrm{j}}/\mathrm{n} \\ \vdots \\ \sum C_{\mathrm{mj}}/\mathrm{n} \end{bmatrix}=\begin{bmatrix} \overline{C_1} \\ \overline{C_2} \\ \vdots \\ \overline{C_m} \end{bmatrix}. \tag{4}$$

(4) Locate the extreme points of the scale series to find the predominant scale needed.

(5) The scales corresponding to the extreme points represent the predominant scales (or cycles) and the specific thickness values can be obtained according to the relationship between scale and frequency in wavelet analysis (see Eq. 5).

$$F_a=\frac{F_c}{a\cdot\Delta}. \tag{5}$$

where a is the scale factor, Δ is the sampling period, F_c is the center frequency of the wavelet, and F_a is the quasi-frequency at a. F_a can be regarded as the real frequency of a within a tolerant error range. F_a can be the number of cycles within a thickness unit if Δ is the sampling interval in thickness. Morlet wavelet is used as the mother wavelet in our study, so F_c = 0.8125 Hz. The reciprocal of F_a is the predominant cycle we want to find.

(6) The number of the sinusoidal wave in the wavelet coefficient at the predominant scale can be counted.

4. RESULTS

4.1. WSSA Results

In this study, the WSSA method was undertaken in the Matlab platform and applied to the Th data series from the studied section. Five extreme points within the scale series have been recognized: $a_1 = 3$, $a_2 = 6$, $a_3 = 19$, $a_4 = 81$, and $a_5 = 114$ (Fig. 3c).

Approximate position of Fig. 3

Periods of the Milankovitch cycles (~20 kyr precession, 40 kyr obliquity, 100 kyr short eccentricity, and 400 kyr long eccentricity) and their duration ratio (~1:2:5:20) are relatively stable in any particular geological interval. Matching the thickness of sedimentary cycles with Milankovitch cycles is a widely accepted method to determine whether the sedimentary unit is affected by the astronomical orbital forces (Hinnov, 2000; Weedon, 2003). According to the method for the recognition of Milankovitch cycles, there are two equally possible matching schemes to fit the Milankovitch syndrome. The first is at the scale of a = 3 (a_1) and a = 6 (a_2), implying a 1:2 ratio, corresponding to the ratio between precession and obliquity cycles. The second is at the scale of a = 19 (a_3) and a = 81 (a_4), implying a 1:4.3 ratio, corresponding to the ratio between precession and short eccentricity cycles. When we enter a = 3 and a = 6 into Equation (5), periodic thicknesses for the precession cycles of 0.18 m and obliquity cycles of 0.37 m are obtained. This would imply a duration for the entire 17 m thick studied section of about 2 Myr. A 2 Myr age range for the studied section conflicts not only with the radio isotope dating results (He et al., 2011), but also with the results of our own paleomagnetic analysis. In the studied section, our palaeomagnetic analysis indicates that only a normal polarity intervals exist, but at no point during the Miocene does a normal polarity interval last as long as 2 Myr (see below). However, when we enter values of a = 19 and a = 81 into Equation (5), periodic thicknesses for the precession cycles of 1.17 m and eccentricity of 4.98 m are obtained, and these values are much more reasonable. In this case, the deposition of the studied section would have taken about 0.3 Myr, equivalent of 15 precession cycles. We therefore conclude that the Th signal at the scale a = 19 and a = 81 reflects the precession and short eccentricity cycles in the Shanwang Formation. The various cycles and their duration of accumulation in terms of precession and eccentricity (a =19 and a = 81) are shown in Figure 4.

Approximate position of Fig. 4

4.2. Results with Parallel Methods

In order to verify the validity of the WSSA method, the Correlation Coefficient (COCO) and Multitaper-Method spectral analysis (MTM) methods were also applied to the detrended Th series to test the robustness of the evidence in our cyclostratigraphic interpretation. These analyses were performed with the computer routine ACycle 0.2.5 (Li et al., 2018). Long-term trend removal was needed in order to avoid distortion of the low-frequency section of the spectrum using a “Lowess smoother” (smoother = 50%). COCO analysis of the detrended Th series of the diatomaceous shale indicates the mean sedimentation rate at 4.8 cm/kyr is the optimal result, the correlation coefficient of which is the largest and exceed the critical significance level (Fig. 5a-c). The MTM power spectrum of the detrended Th series from the diatomaceous shale shows an obvious peak of 5.06 m (Fig. 5d), which is consistent well with the cycles recognized by our WSSA method (4.98 m). Combined with the sedimentation rate (4.8 cm/kyr) determined from the COCO analysis, the cycle of 5.06 m is concluded as representing the short eccentricity cycle (105 kyr). Unfortunately, the peaks of 0.83 m and 1.12 m (representing the precession cycle based on the sedimentation rate of 4.8 cm/kyr) are distinguishable but with a low value; confidence levels of these spectral peaks show minor values below 90%. This is a common phenomenon for which possible reasons for the low confidence levels include variations in accumulation rate, bioturbation, undetected hiatuses, or the possibility that a precession signal is not actually present in the Th series (Weedon, 2003). Overall, this result is consistent with the cycles recognized by our WSSA method. Slight differences in the average deposition rates (4.8 cm/kyr by COCO and 5.7 cm/kyr by WSSA) may be due to different mathematical algorithms. This is an uncommonly high sedimentation rate, but is not exceptional for lacustrine settings. A high sedimentation rate for the Shanwang Formation has previously been postulated by other researchers (e.g., Tian et al., 2015) on the basis of the extremely good preservation of the fossils, enhancing their preservation potential through sedimentary obrution (rapid burial or smothering event).

By comparison, it was found that the same results can be reached by both the WSSA and parallel methods, and there are fewer redundant peaks in the WSSA results for final selection. Furthermore, it is easier to implement WSSA method as no additional routine packages required to undertake the analysis.

Approximate position of Fig. 5

5. PALEOMAGNETIC ANALYSIS

In addition to the cyclostratigraphic analysis, we investigated whether the age data thus obtained for the deposition of unit 2 of the Shanwang Formation fits with the established paleomagnetic context of the Miocene. A detailed paleomagnetic survey was carried out on the basis of 93 oriented samples with a size of 30 cm × 23 cm × 30 cm, which had a total weight of ~3 tons and spanned almost the entire section under study. Samples were collected using an electric saw. As the tectonic dip of the Shanwang Formation is less than 5°, implying a near-horizontal position, the orientation of the samples could be marked by indicating the direction of the magnetic North Pole on the bedding surface of each sample.

From the 93 samples, 31 fairly evenly spaced specimens were selected; these were cut into 167 smaller oriented pieces with sizes of 2 cm × 2 cm × 2 cm each for geomagnetic measurements. The measurements were performed in the Paleomagnetism and Geochronology Laboratory (SKL-LE) of the Institute of Geology and Geophysics, Chinese Academy of Sciences. Systematic demagnetization of all samples was done using a three-axes low-temperature superconducting magnetometer 2G760 and a stepwise progressive alternating demagnetization method. The twelve demagnetization intensity steps were set at 0, 5, 10, 15, 20, 25, 30, 40, 50, 60, 70, 80 mT. The original demagnetization data were converted with data conversion tools, then processed with PMGSC4.2 software and finally presented in terms of the Zijderveld graphic method. The demagnetization curves of most of these samples were found to yield a stable and reliable character remanence at the fifth demagnetization step (20 mT). The declination and inclination curves of the effective samples show that the entire profile of the diatomaceous shale part of the Shanwang Formation has a normal polarity with stable declination and inclination (Fig. 6).

Approximate position of Fig. 6

6. CHRONOSTRATIGRAPHIC IMPLICATIONS

We combined the above geomagnetic polarity result with the results from Fang et al. (1980) to construct a geomagnetic polarity column (Fig. 7, middle). This presents, from bottom to top, the lower part of the Niushan Formation with a normal polarity (N1), the upper part of the Niushan Formation with a reversed polarity (R1), the main part of the Shanwang Formation with a normal polarity (N2), the top part of the Shanwang Formation with a reversed polarity (R2), and the Yaoshan Formation with a normal polarity (N3).

Approximate position of Fig. 7

Constrained by the $^{40}Ar/^{39}Ar$ dating results of He et al. (2011) (Fig. 7, left), who attributed an age of 17.3±1.4 Ma to the lower part of the Yaoshan Formation, an age of 17–18 Ma to the lower part of the Shanwang Formation, and an age of 21.0±2.5 Ma to the top of the Niushan Formation, the Shanwang Formation can be correlated with the international GPTS (Ogg, 2012) (Fig. 7, right). It was thus found that there are only two reasonable matching modes, that is, matching N2 with either subchron 5Dn or subchron 5En of Chron 5 (Fig. 7). Considering that the duration of 0.298 Myr of subchron 5Dn is shorter than the above WSSA results of the studied section, we consider it appropriate to correlate N2 in the Shanwang Formation with subchron 5En. This implies that deposition of the Shanwang Formation started about 18.5 Ma (Fig. 7).

According to Gradstein and Ogg (2004), the Early Miocene comprises the Aquitanian and Burdigalian stages, whereas the Middle Miocene comprises the Langhian and Serravallian stages, and the Late Miocene the Tortonian and Messinian stages. Using the current radiometric stage ages (GTS 2018), the Early Miocene lasted from 23.03 to 15.97 Ma, the Middle Miocene from 15.97 to 11.63 Ma, and the Late Miocene from 11.63 to 5.33 Ma (Cohen et al., 2013: updated in 2018-08). Consequently, the Shanwang Formation must have formed during the later part of the Early Miocene during the Burdigalian stage, and not during the Middle Miocene as previously suggested (Sun et al., 2002; Liang et al., 2003; Zbynek Rocek et al., year). In this stratigraphic context, the Shanwang lagerstätte biota therefore predates the Middle Miocene Climate Optimum (MMCO), in which the initial warming began ca. 18 Ma (Harris et al., 2017) with a peak at ca. 17–14.75 Ma (Zachos et al., 2001). It was therefore not deposited during the onset or main period of the MMCO as previously considered (e.g., He et al., 2011). However, we note that different age ranges for the MMCO have previously been published, including estimates of 16–14 Ma (Song et al., 2018), 16–14.8 Ma (Flower and Kennett, 1994) and 17–15 Ma (Wan et al., 2009). With deposition of the studied section starting at approx. 18.5 Ma and lasting 0.3 Myr, we conclude that the Shanwang Formation predates each of these estimates for the MMCO.

According to recent research the age range of European Mammalian Zone MN4 is from 17.2–16.4 Ma and the age range of MN3 is ca. 19.5–17.2 Ma (Jovells and Casanovas, 2018). This is not very different from the ages determined by Larrasoaña et al. (2006) who located the upper boundary of MN3 at 16.8–17 Ma, and the lower boundary of MN3 at ca. 20.1 Ma. We conclude that the biota in the Shanwang Formation should be correlated stratigrpahically to European Mammalian Zone MN3, rather than to MN5 or MN4 as suggested by Deng et al. (2003).

7. CONCLUSIONS

Our detailed cyclostratigraphic study based on thorium data shows that the sedimentation of the Miocene diatomaceous shale in the Shanwang Basin was driven by the precession and short eccentricity astronomical cycles. A total of three short eccentricity and fifteen precession cycles have been identified. The studied interval of the succession can be estimated to have lasted 0.3 Myr with a depositional rate of about 5.7 cm/kyr. Paleomagnetic analysis limited the formation time of the Shanwang Formation to 18.5 Ma, giving a non-floating geologic time scale of the succession with a resolution as high as 20 kyr. Based on these results, we think that the Shanwang lagerstätte biota was not deposited during the onset or main period of the Middle Miocene Climate Optimum (MMCO), but was deposited ahead of it.

The Wavelet Scale Series Analysis (WSSA) method derived from the so called ‘mathematical microscope’ wavelet analysis can overcome the redundancy of CWT in recognizing the predominant periodicity within one-dimensional signals and serve as a practical solution for identifying Milankovitch cycles from geologic time series. .

ACKNOWLEDGEMENTS

Thanks are given to Professor A.J. (Tom) Van Loon for his constructive suggestions on an earlier version of the manuscript. Thanks are also given to Mr. Gang Zhao for his help in the field. This work was financially supported by the National Natural Science Foundation of China (41472092) and the Scientific and Technological Innovation Project of the Qingdao National Laboratory for Marine Science and Technology (No. 2016ASKJ13).

REFERENCES

Aigner, T., Schauer, M., Junghans, W.D., and Reinhardt, L., 1995, Outcrop gamma-ray logging and its applications: examples from the German Triassic. Sedimentary Geology, 100, 47–61.

Batenburg, S.J., Sprovieri, M., Gale, A.S., Hilgen, F.J., Hüsing, S., Laskar, J., Liebrand, D., Lirer, F., Orue-Etxebarria, X., Pelosi, N., and Smit, J., 2012, Cyclostratigraphy and astronomical tuning of the Late Maastrichtian at Zumaia (Basque country, Northern Spain). Earth and Planetary Science Letters, 359–360, 264–278.

Chui, C.K., 1992, Wavelets: A tutorial in theory and applications. Academic Press, San Diego, 723 p.

Cohen, K.M., Finney, S.C., Gibbard, P.L., and Fan, J.-X., 2013, The ICS international chronostratigraphic chart. Episodes, 36, 199–204.

Deng, T., Wang, W.M., and Yue, L.P., 2003, Recent advances of the establishment of the Shanwang stage in the Chinese Neogene. Vertebrata Palasiatica, 41, 314–323. (in Chinese with English abstract)

Dimri, V.P., and Prakash, M.R., 2001, Scaling of power spectrum of extinction events in the fossil record. Earth and Planetary Science Letters, 186, 363–370.

Fang, D.J., Zhu, X.Y., He, L.Z., and Lu, Y.S., 1980, The study of palaeomagnetism in Cainozoic basalts and its strata meaning at San-Huang District, San-Tung. Journal of Zhejiang University, S1, 49–57. (in Chinese with English abstract)

Flower, B.P., and Kennett, J.P., 1994, The middle Miocene climatic transition-East Antarctic ice-sheet development, deep-ocean circulation and global carbon cycling. Palaeogeography, Palaeoclimatology, Palaeoecology, 108, 537–555.

Ghil, M., Allen, M.R., Dettinger, M.D., Ide, K., Kondrashov, D., Mann, M.E., Robertson, A.W., Saunders, A., Tian, Y., Varadi, F., and Yiou, P., 2002, Advanced spectral methods for climatic time series. Reviews of Geophysics, 40, 1003.

Gradstein, F., and Ogg, J., 2004, Geologic Time Scale 2004 - why, how, and where next!. Lethaia, 37, 175–181.

Harris, E.B., Strömberg, C.A.E., Sheldon, N.D., Smith, S.Y., and Vilhena, D.A., 2017, Vegetation response during the lead-up to the middle Miocene warming event in the Northern Rocky Mountains, USA. Palaeogeography, Palaeoclimatology, Palaeoecology, 485, 401–415.

He, H.Y., Deng, C.L., Pan, Y.X., Deng, T., Luo, Z.H., Sun, J.M., and Zhu, R.X., 2011, New ^{40}Ar/^{39}Ar dating results from the Shanwang Basin, eastern China: Constraints on the age of the Shanwang Formation and associated biota. Physics of the Earth and Planetary Interiors, 187, 66–75.

Hilgen, F.J., Kuiper, K.F., and Lourens, L.J., 2010, Evaluation of the astronomical time scale for the Paleocene and earliest Eocene. Earth and Planetary Science Letters, 300, 139–151.

Hinnov, L.A., 2000, New perspectives on orbitally forced stratigraphy. Annual Review of Earth and Planetary Science, 28, 419–475.

Hinnov, L.A., and Goldhammer, R.K., 1991, Spectral analysis of the middle Triassic Latemar Limestone. Journal of Sedimentary Research, 61, 1173–1193.

Hinnov, L.A., and Ogg, J.G., 2007, Cyclostratigraphy and the astronomical time scale. Stratigraphy, 4, 239–251.

Holden, C., 2001, Fossil trove preserved. Science, 291, 1481.

Husson, D., Galbrun, B., Laskar, J., Hinnov, L.A., Thibault, N., Gardin, S., and Locklair, R.E., 2011, Astronomical calibration of the Maastrichtian (Late Cretaceous). Earth and Planetary Science Letters, 305, 328–340.

James, G., and Michael, E.G., 2006, Wavelet extractor: A Bayesian well-tie and wavelet extraction program. Computers and Geosciences, 32, 681–695.

Jovells, V.S., and Casanovas, V.I., 2018, A review of the genus Melissiodon (Cricetidae, Rodentia) in the Vallés-Penedès Basin (Catalonia). Journal of Vertebrate Paleontology, 38, e1520714 (1–9).

Larrasoaña, J.C., Murelaga, X., and Garcés, M., 2006, Magnetobiochronology of Lower Miocene (Ramblian) continental sediments from the Tudela Formation (western Ebro basin, Spain). Earth and Planetary Science Letters, 243, 409–423.

Li, C.K., Wu, W.Y., and Qiu, Z.D., 1984, Chinese Neogene: subdivision and correlation. Vertebrata PalAsiatica, 22, 163–178. (in Chinese with English abstract)

Li, F.L., 1991, Reconsideration of the Shanwang Formation, Linqu, Shandong. Journal of Stratigraphy, 15, 123–129. (in Chinese with English abstract)

Li, M.S., Kump, L. R., Hinnov, L. A., and Mann, M. E., 2018, Tracking variable sedimentation rates and astronomical forcing in Phanerozoic paleoclimate proxy series with evolutionary correlation coefficients and hypothesis testing. Earth and Planetary Science Letters, 501, 165–179.

Liang, M.M., Bruch, A., Collinson, M., Mosbrugger, V., Li, C.S., Sun, Q.G., and Hilton, J., 2003, Testing the climatic estimates from different palaeobotanical methods: an example from the Middle Miocene Shanwang flora of China. Palaeogeography, Palaeoclimatology, Palaeoecology, 198, 279–302.

Mallat, S.G., 1989, A theory for multiresolution signal decomposition: the wavelet representation.

IEEE Transactions on Pattern Analysis and Machine Intelligence, 11, 674–693.

Ogg, J.G., 2012, Geomagnetic polarity time scale. In: Gradstein, F.M., Ogg, J.G., Schmitz, M., Ogg, G. (eds.), The Geologic Time Scale 2012. Elsevier, Amsterdam, p. 85–113.

Osmond, J.K., and Ivanovich, M., 1992, Uranium-series mobilisationand surface hydrology. In: Ivanovich, M., Harmon, R.S. (Eds.), Uranium-series Disequilibrium: Applications to Earth,Marine and Environmental Sciences. Clarendon Press, Oxford, p. 259–289.

Paillard, D., Labeyrie, L., and Yiou, P., 1996, Macintosh program performs time-series analysis. Eos, Transactions American Geophysical Union, 77, 379.

Park, J., and Herbert, T.D., 1987, Hunting for paleoclimatic periodicities in a geologic time-series with an uncertain time scale. Journal of Geophysical Research-Solid Earth, 92, 14027–14040.

Parkinson, D.N., 1996, Gamma-ray spectrometry as a tool forstratigraphical interpretation: examples from the western European Lower Jurassic. In: Hesselbo, S.P., Parkinson, D.N. (Eds.), Sequence Stratigraphy in British Geology, Geological Society Special Publication, vol. 103, p. 231–255.

Pas, D., Hinnov, L., Day, J.E., Kodama, K., Sinnesael, M., and Liu, W., 2018, Cyclostratigraphic calibration of the Famennian stage (Late Devonian, Illinois Basin, USA). Earth and Planetary Science Letters, 488, 102–114.

Prokoph, A., and Agterberg, F.P., 1999, Detection of sedimentary cyclicity and stratigraphic completeness by wavelet analysis: an application to Late Albian cyclostratigraphy of the western Canada sedimentary basin. Journal of Sedimentary Research, 60, 862–875.

Prokoph, A., and Agterberg, F.P., 2000, Wavelet Analysis of Well-Logging Data from Oil Source Rock, Egret Member, Offshore Eastern Canada. American Association of Petroleum Geologists Bulletin, 84, 1617–1632.

Prokoph, A., and Barthelmes, F., 1996, Detection of nonstationarities in geological time series: wavelet transform of chaotic and cyclic sequences. Computers and Geosciences, 22, 1097–1108.

Qin, W.S., Liu, J.B., Han, B.F., Wang, X.Z., and Li, F.C., 2004, Types and origin of diatomaceous laminae of the Miocene Shanwang Formation in Linqu, Shandong Province. Acta Sedimentologica Sinica, 22, 267–275. (in Chinese with English abstract)

Seilacher, A., Reif, W.E., and Westphal, F., 1985, Sedimentological, ecological and temporal patterns of fossil Lagerstätten. Philosophical transactions of the Royal Society of London. Series B, Biological Sciences, 311, 5–24.

Song, Y.G., Wang, Q.S., An, Z.S., Qiang, X.K., Dong, J.B., Chang, H., Zhang, M.S., and Guo, X.H., 2018, Mid-Miocene climatic optimum: Clay mineral evidence from the red clay succession, Longzhong Basin, Northern China. Palaeogeography, Palaeoclimatology, Palaeoecology, 512, 46–55.

Sun, Q.G., Collinson, M.E., Li, C.S., Wang, Y.F., and Beerling, D.J., 2002, Quantitative reconstruction of palaeoclimate from the Middle Miocene Shanwang flora, eastern China. Palaeogeography, Palaeoclimatology, Palaeoecology, 180, 315–329.

Tagliaferri, R., Ciaramella, A., Longo, G., Milano, M., Barone, F., and Pelosi, N., 2001, Soft computing methodologies for spectral analysis in cyclostratigraphy. Computers and Geosciences, 27, 535–548.

Thomson, D.J., 1982, Spectrum estimation and harmonic analysis. Proceedings of the IEEE, 70, 1055–1096.

Tian, H.S., Van Loon, A.J.(Tom), Zhang, Z.Q., Zhang, S.H., Zhang, B.H., Lu, M.Y., Li, F.C., and Ma, X.M., 2015, Neogene Paleoseismic Events and the Shanwang Biota's Burial in the Linqu Area, Shandong Province, China. Acta Geologica Sinica (English edition), 89, 1103–1119.

Torrence, C., and Compo, G.P., 1998, A Practical Guide to Wavelet Analysis. Bulletin of the American Meteorological Society, 79, 61–78.

Wan, S., Kürschner, W.M., Clift, P.D., Li, A., and Li, T., 2009, Extreme weathering/erosion during the Miocene Climatic Optimum: evidence from sediment record in the South China Sea. Geophysical Research Letters, 36, L19706.

Wang, C.S., Scott, R.W., Wan, X.Q., Graham, S.A., Huang, Y.J., Wang, P.J., Wu, H.C., Dean, W.E., Zhang, L.M., 2013, Late Cretaceous climate changes recorded in Eastern Asian lacustrine deposits and North American Epieric sea strata. Earth-Science Reviews, 126, 275–299.

Weedon, G.P., 1986, Hemipelagic shelf sedimentation and climatic cycles: the basal Jurassic (Blue Lias) of South Britain. Earth and Planetary Science Letters, 76, 321–335.

Weedon, G.P., 1989, The detection and illustration of regular sedimentary cycles using Walsh power spectra and filtering, with examples from the Lias of Switzerland. Journal of the Geological Society, 146, 133–144.

Weedon, G.P., 2003, Time-Series Analysis and Cyclostratigraphy. Cambridge University Press, Cambridge, p. 1–259.

Wu, H.C., Zhang, S.H., Hinnov, L.A., Jiang, G.Q., Yang, T.S., Li, H.Y., Wan, X.Q., and Wang, C.S., 2014, Cyclostratigraphy and orbital tuning of the terrestrial upper Santonian-Lower Danian in Songliao Basin, northeastern China. Earth and Planetary Science Letters, 407, 82–95.

Wu, H.C., Zhang, S.H., Jiang, G.Q., and Huang, Q.H., 2009, The floating astronomical time scale for the terrestrial Late Cretaceous Qingshankou Formation from the Songliao Basin of Northeast China and its stratigraphic and paleoclimate implications. Earth and Planetary Science Letters, 278, 308–323.

Wu, H.C., Zhang, S.H., Jiang, G.Q., Hinnov, L., Yang, T.S., Li, H.Y., Wan, X.Q., and Wang, C.S., 2013, Astrochronology of the Early Turonian–Early Campanian terrestrial succession in Songliao Basin, northeastern China and its implication for the long-period behavior of the Solar System. Palaeogeography, Palaeoclimatology, Palaeoecology, 385, 55–70.

Yang, H., and Yang, S.P., 1994, The Shanwang fossil biota in eastern China: a Miocene konservat lagerstätte in lacustrine deposits. Lethaia, 27, 345–354.

Yu, J.F., Guo, K., Yuan, X.X., Fu, W.Z., and Xun, Z.F., 2010, Wavelet denoising of well logs and its geological performance. Energy Exploration and Exploitation, 28, 87–95.

Yu, J.F., Sui, F.G., Li, Z.X., Liu, H., and Wang, Y.L., 2008, Recognition of Milankovitch cycles in the stratigraphic record: application of the CWT and the FFT to well-log data. Journal of China University of Mining and Technology, 18, 594–598.

Yu, J.F., Zhao, X.G., Pang, X.L., Hilton, J., Fu, W.Z., Zhao X.L., Song, Z.J., Hu, J.L., Lu, L., Zhang, H.J., Yang, Z.Q., Qiao, W.Y., and Shi, S., 2017, Redefining the age of the Cenozoic Shanwang Formation in Shanwang Basin. Acta Geologica Sinica (English edition), 91, 1491–1492.

Zachos, J., Pagani, M., Sloan, L., Thomas, E., and Billups, K., 2001, Trends, rhythms, and aberrations in global climate 65 Ma to present. Science, 292, 686–693.

Zhang, L.M., Wang, C.S., Li, X.H., Cao, K., Song, Y., Hu, B., Lu, D.W., Wang, Q., Du, X.J., and Cao, S., 2015, A new paleoclimate classification for deep time. Palaeogeography, Palaeoclimatology, Palaeoecology, 443, 98–106.

Zhang, M.S., and Shan, L.F., 1994, Sedimentary Geology of Shanwang Basin. Geological Publishing House, Beijing, 84 p.

Zhang, X.L., Feng, Q., Sun, P., and Li, W., 2010, Characteristics of high gamma ray reservoir of Yanchang formation in Ordos basin. Chinese Journal of Geophysics, 53, 205–213.

FIGURES

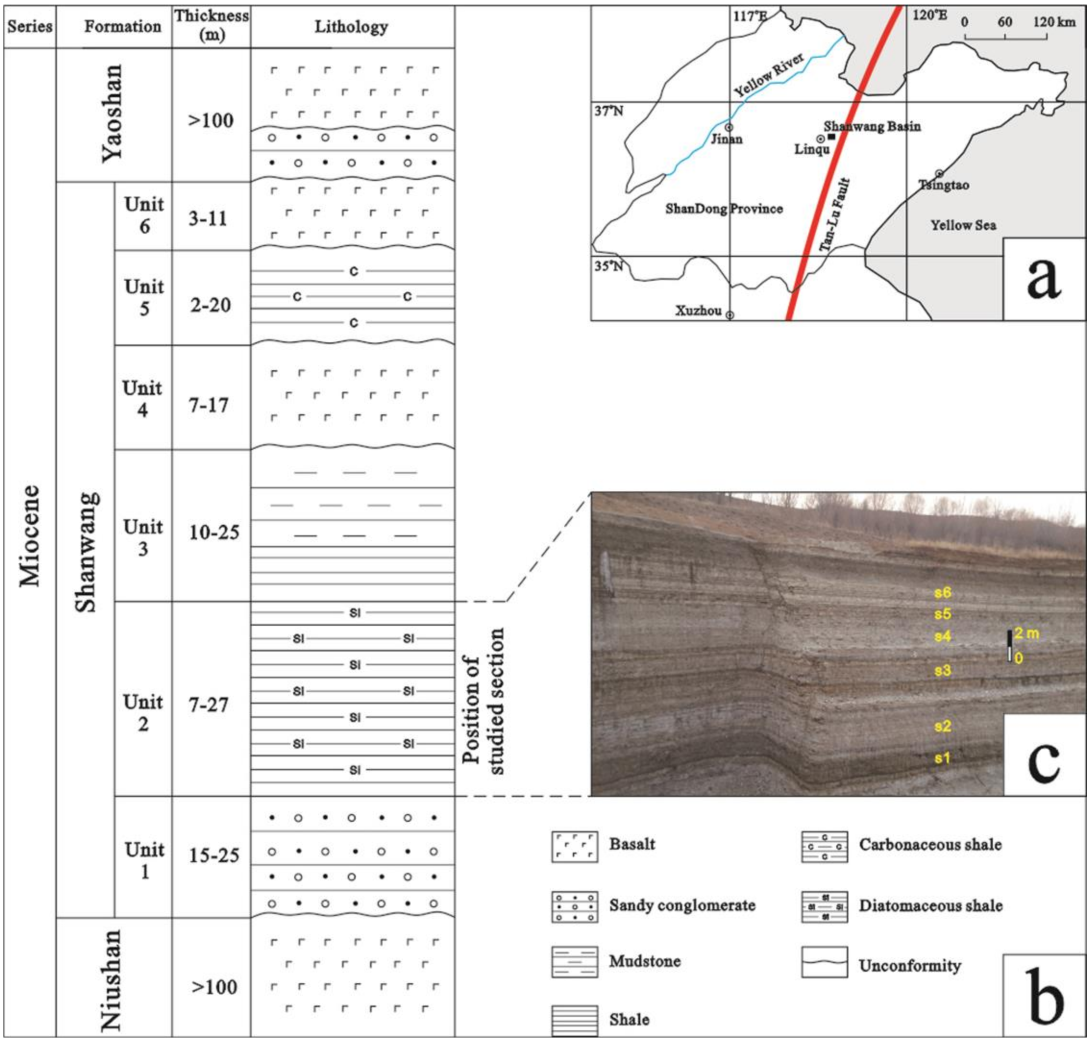

Fig. 1. (a) Location of the Shanwang Basin in Shandong Province (E. China). (b) Sedimentary succession of the Shanwang Formation in Linqu (modified from the Fourth Geological Prospecting Institute of Shandong 2002 and Liang et al., 2003). (c) Outcrops of the studied section. s1-s6: positions of the samples from which the thin sections in Fig. 2 were prepared.

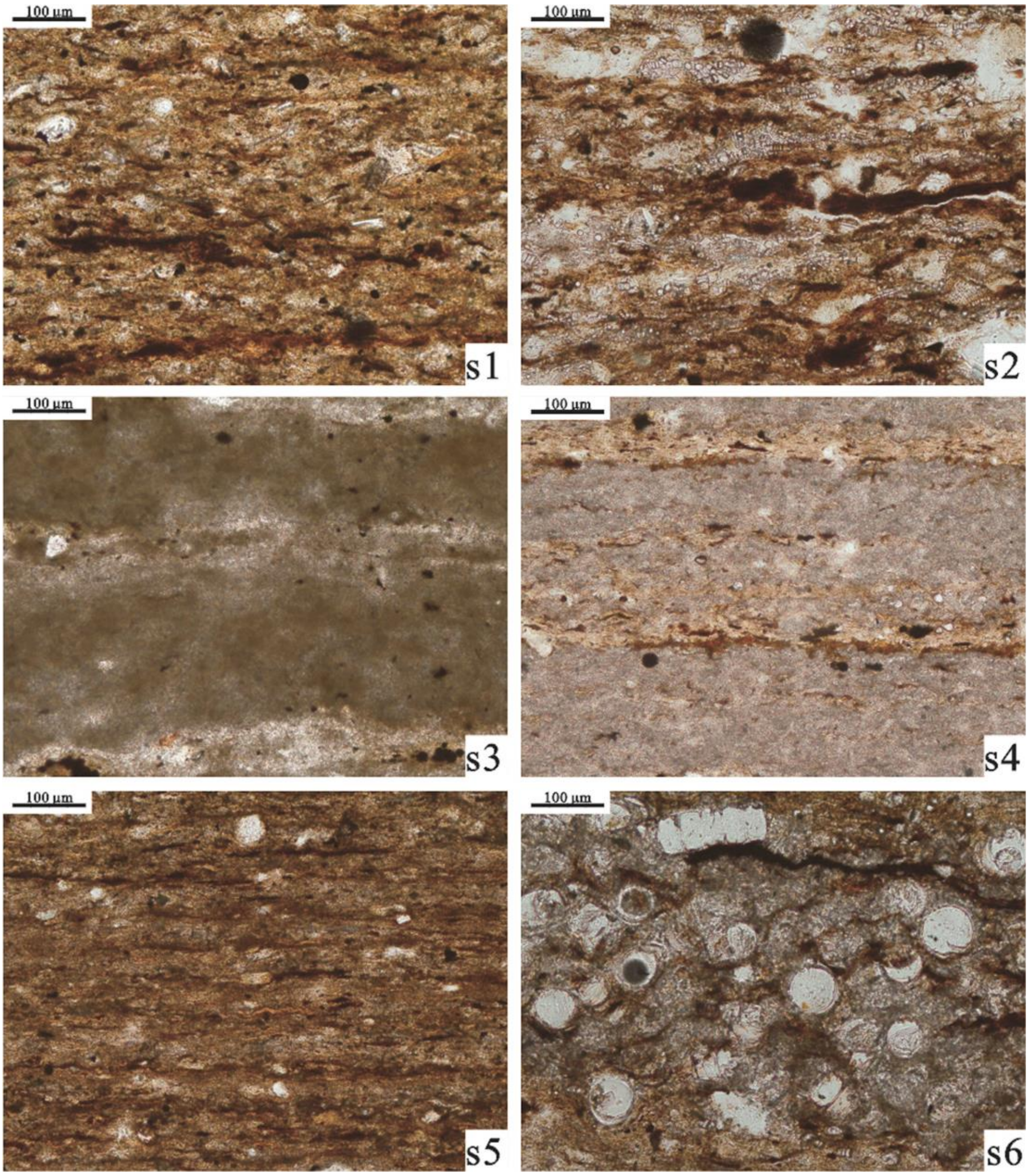

Fig. 2. Thin section photomicrographs of the diatomaceous shales in plane polarized transmitted light. (s1) Dark clay layer with small amount of bright diatoms. (s2) Bright diatom layer with small amount of clay. (s3) Thick layer of dark organic matter with thin layer of bright diatom. (s4) Thick layer of bright diatom with thin layer of dark clay. (s5) Dark clay layer with small amount of bright diatoms. (s6) Bright diatom layer with small amount of clay. For sample locations, see Fig. 1.

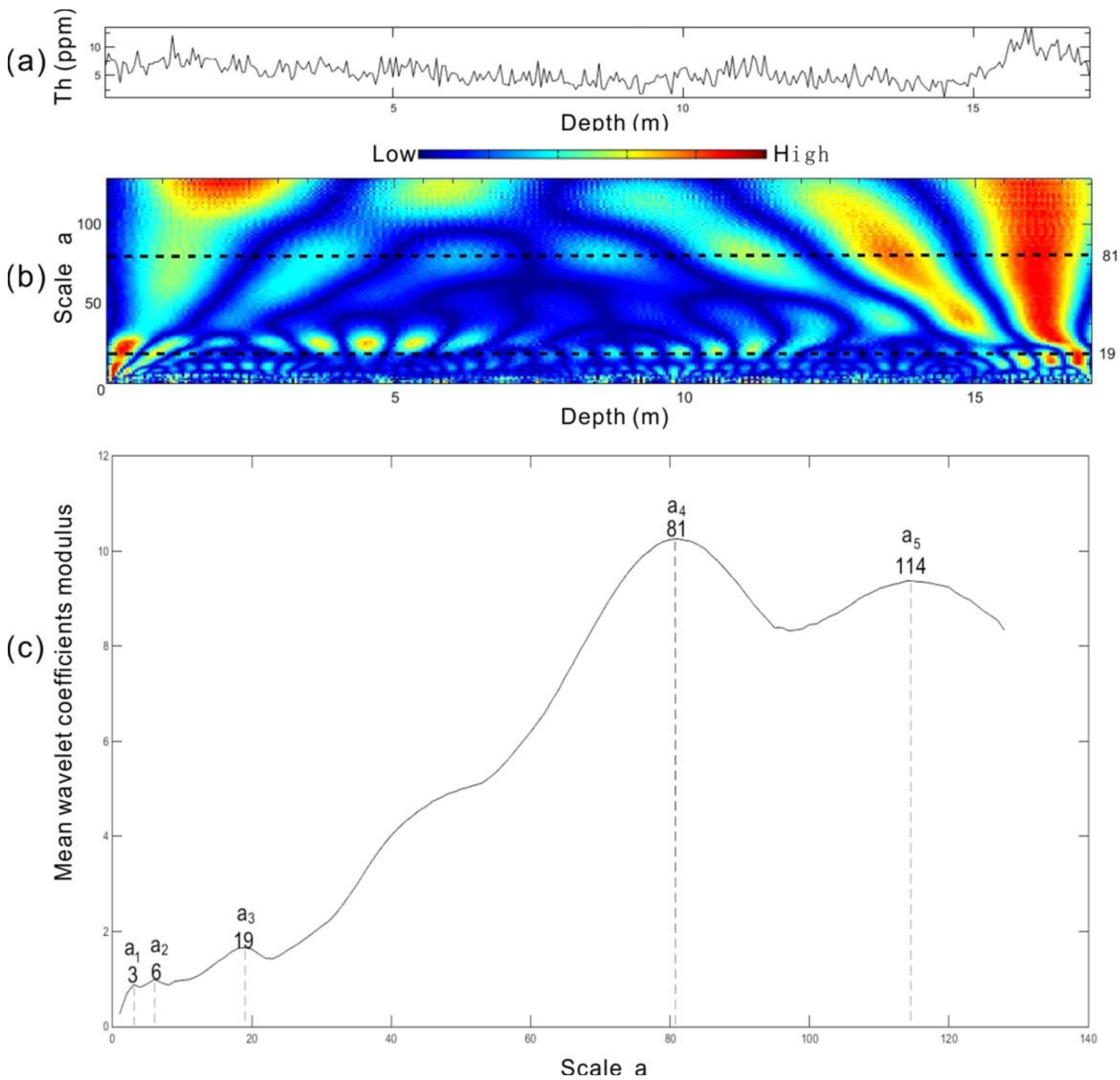

Fig. 3. WSSA result. (a) Raw thorium (Th) (in ppm) data. (b) CWT scalogram of the Th series in the studied section. The blue color represents low values and red high values for the wavelet coefficents at different scale and depth. (c) Wavelet scale series curve of the Th series in the studied section.

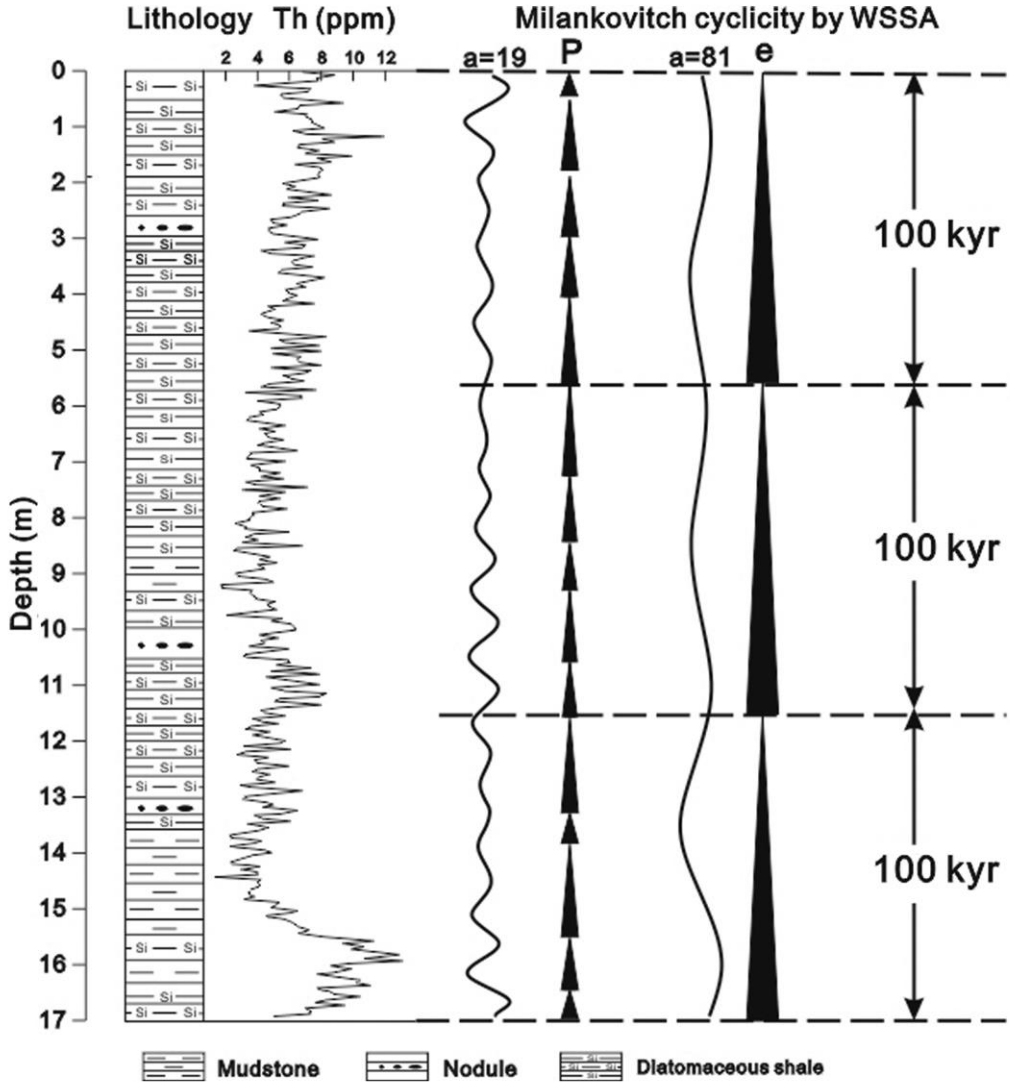

Fig. 4. Sedimentary log of the studied section with concentration of thorium (Th) (in ppm) and corresponding Milankovitch cyclicity by WSSA.

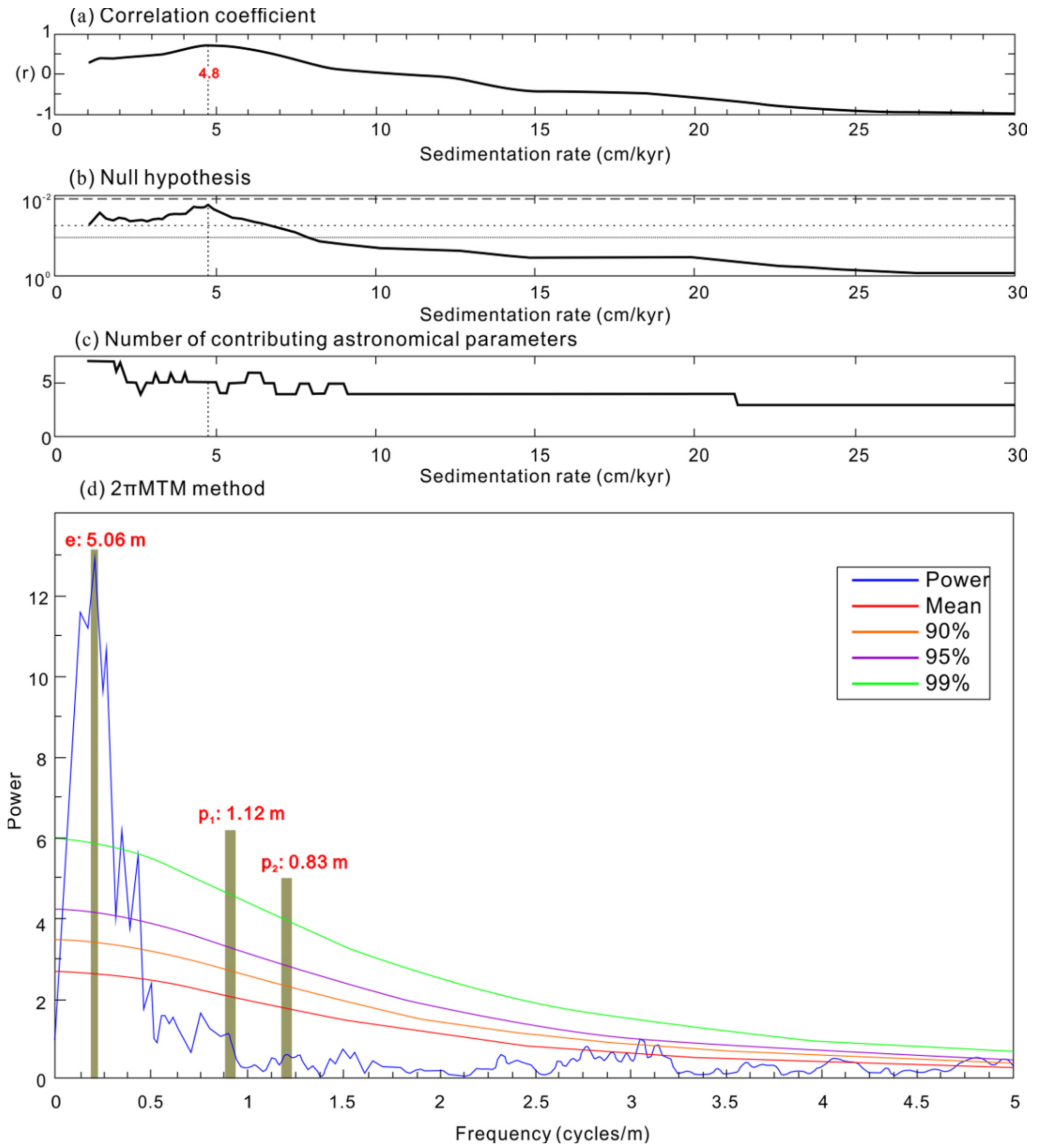

Fig. 5. 2-slice COCO analysis and 2πMTM power spectra of the detrended Th series in the studied section. (a) COCO spectra shown with mean sedimentation rate at 4.8 cm/kyr. (b) H_0 significance level for the COCO results. (c) Number of contributing astronomical parameters. The target astronomical series using La04 solution at 18 Ma (Laskar et al., 2004). The number of Monte Carlo simulations is 2000. Sedimentation rates range from 1 to 30 cm/kyr with a step of 0.1 cm/kyr. (d) MTM spectra of the detrended Th series shows peaks of 5.06m, 1.12m and 0.83m, which are interpreted to represent short eccentricity (e) and precession (p).

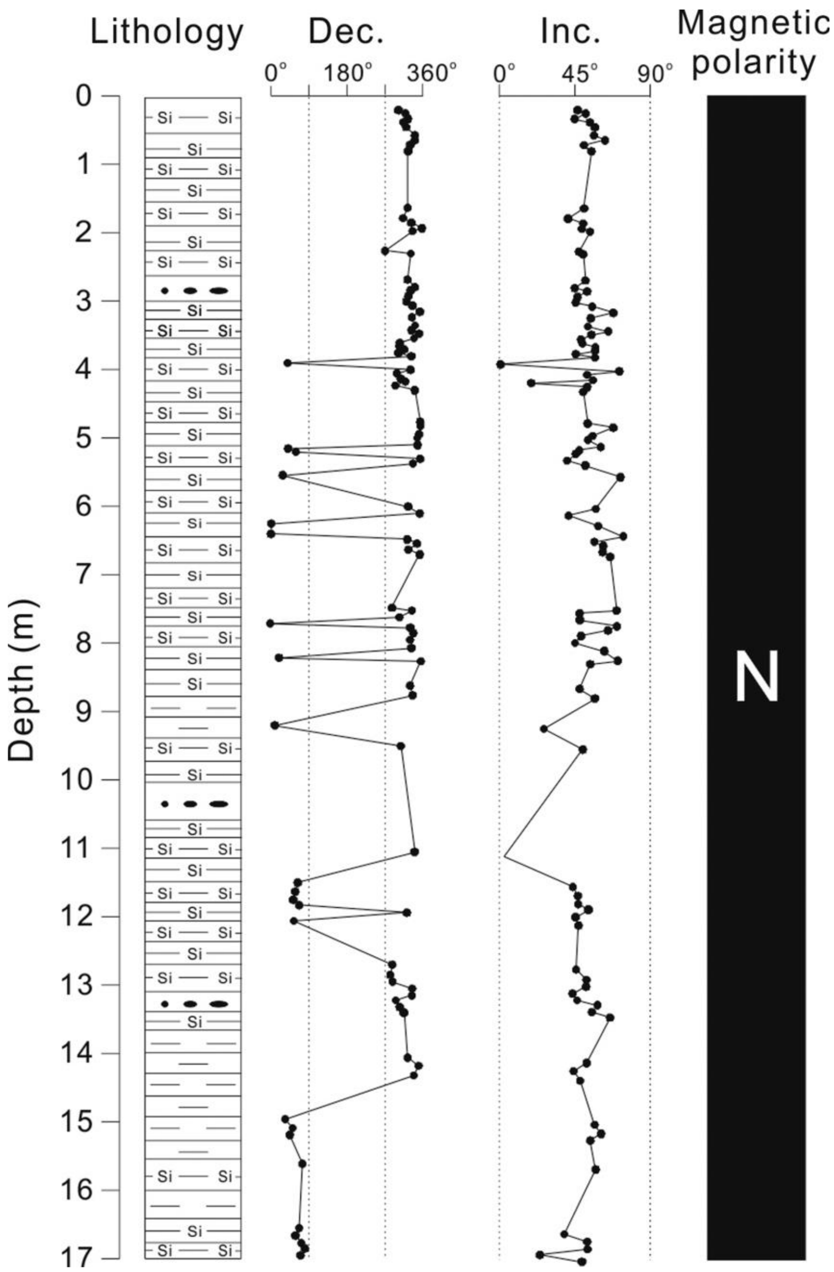

Fig. 6. Result of paleomagnetic analysis of the section under study. dec = declination; inc = inclination.

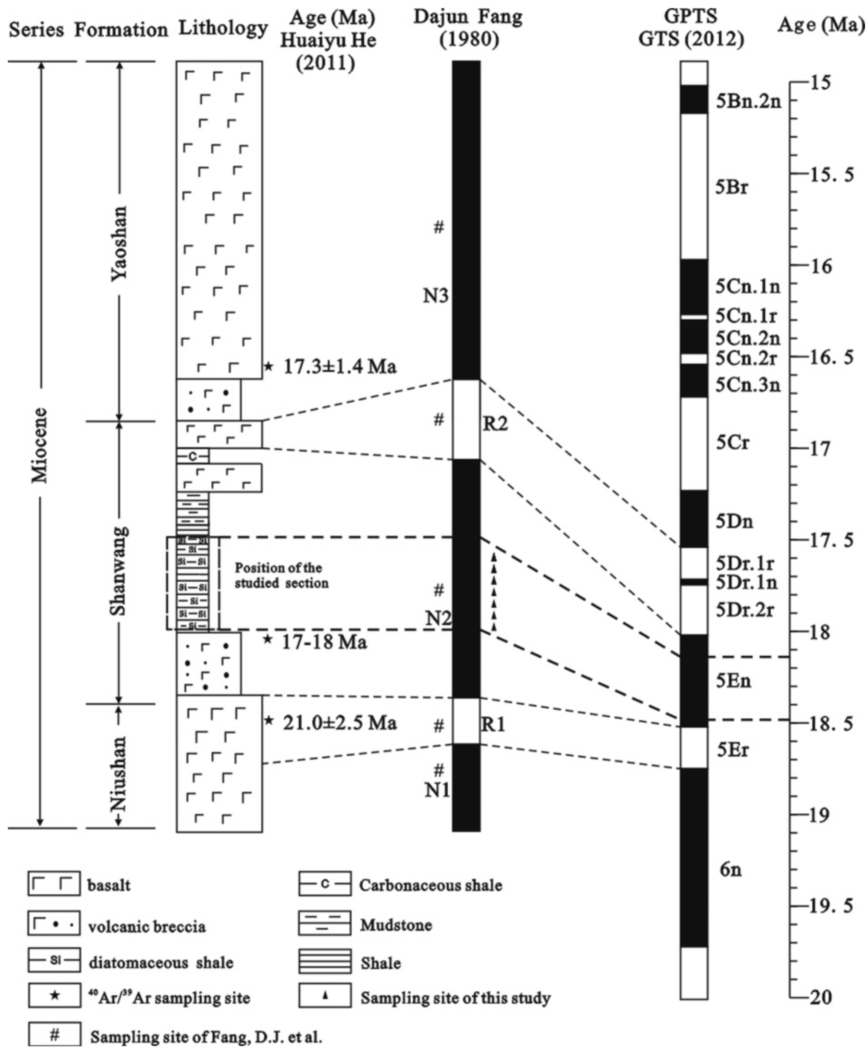

Fig. 7. Age of the Shanwang Formation constrained by radiometric dating and geomagnetic data.